

# NANOPARTICLE AND NANOTUBE MODIFIED ELECTRODES: THE RESPONSE OF DROP CASTED SURFACES

Yifei Zhang<sup>1</sup>, Archana Kaliyaraj Selva Kumar<sup>1</sup>, Dr. Danlei Li, Dr. Minjun Yang, Prof. Dr. Richard G. Compton\*

*Physical and Theoretical Chemistry Laboratory, Department of Chemistry, University of Oxford, South Parks Road, Oxford OX1 3QZ, United Kingdom*

## Abstract

The morphology of electrodes modified by drop casting layers of multi-walled carbon nanotubes (MWCNTs) and platinum nanoparticles (PtNPs) is investigated and shown to exhibit significant heterogeneity both in the form of 'patchy' surfaces and of 'coffee rings' formed after evaporation of the carrier solvent. The variation of the heterogeneity with total average coverage is studied and the consequences for quantitative analytical voltammetry assessed. Specifically the oxidation of bromide in aqueous solution is examined in the case of MWCNT modified electrodes and the oxidation of aqueous As(III) in that of PtNPs modified electrodes. In both cases, significant deviations from the expected voltammetry are observed even for average coverages which correspond to much in excess of a monolayer of CNTs or NPs. The observed voltammetry is related to the observed structure and the use of such modified electrodes, without concomitant microscopic surface characterisation, is caveated.

.....  
Keywords: *nanoparticles, nanotubes, particle modified electrodes (PMEs), drop-casted films, electro-catalysts, coffee ring effect.*

\* Corresponding author.

Email address: [Richard.compton@chem.ox.ac.uk](mailto:Richard.compton@chem.ox.ac.uk) (R. G. Compton)

1. These authors contributed equally to this work.

## Introduction

The modification of electrode surfaces with drop-casted layers of particles such as nanotubes or nanoparticles represents a popular approach to amperometric electrochemical sensing <sup>[1]</sup>. The aim of the modification and the creation of particle modified electrodes (PMEs) is usually to impart greater apparent electrocatalytic behaviour to the surface so that the oxidation or reduction of the target analyte occurs at lower potentials, and ideally with larger currents, than seen at the 'naked' (or 'bare') electrode so minimising the impact of otherwise interfering species and offering greater analytical sensitivity. Such decreases of overpotential can result from a diversity of effects including changed interfacial electron transfer kinetics, altered mass transport and analyte adsorption effects.

The first of these effects are expected, since the sensitivity of electron transfer to the chemical and physical nature of the electrode is widely recognized especially in multistep processes where high energy intermediates can adsorb and so stabilize on some surfaces. Both the hydrogen evolution reaction (HER) <sup>[2]</sup> and the oxygen reduction reaction (ORR) <sup>[3]</sup> are paradigm cases with extremes of behaviour noted. Implicit in the idea that the modified layer(s) might change the electron transfer kinetics is the requirement that the particles are electrically conductive and that the electron transfer with the analyte takes place at the particle-solution interface (as opposed to at the substrate electrode). If, in contrast, the particle is non-conductive then a shift and amplification of the analyte signal is possible if there is marked adsorption (and hence pre-concentration) of the target on the particle surfaces which may also provide an enhanced surface area on which adsorption can take place. The increased amount of the target close to the electrode surface clearly benefits the analytical sensitivity

with the assumed insulating character of the particles, which dictates that the charge transfer likely occurs at the substrate after desorption. However, there is a ‘trade off’ between the requirements of a strong adsorption leading to a high local concentration and for the accumulated materials to be facily released in response to a potential applied to the electrode <sup>[4]</sup>. This trade-off results in only a limited enhancement of the target current in the case of amperometric sensing <sup>[4]</sup>.

In the case of the particle modification altering the mass transport to an electrode then again a distinction must be drawn between the case of, on the one hand, conductive particles which themselves act as the centres for electrolysis and, on the other hand, of non-conductive particles. A further key controlling factor is the extent of the coverage of the particles, which can range from sub-monolayer at one extreme through to a thin, porous layer at the other and thus reflect both the coverage and the conductivity, four limiting cases emerge.

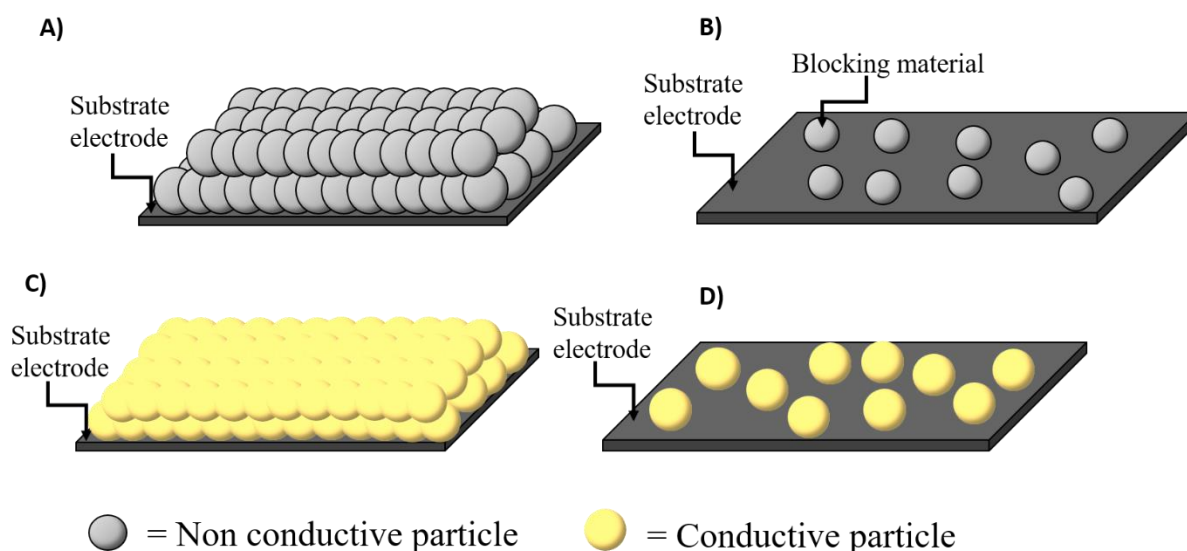


**Figure 1.** Schematic representation of substrate electrode and drop cast particles illustrating Cases A, B, C and D (see text).

**Case A** This case is that of a thick, porous layer of non-conductive particles with the site of electrolysis at the surface of the substrate electrode. Here the effect of the layer is typically to reduce the magnitude of the current as compared to that seen at the corresponding bare substrate electrode <sup>[5]</sup>. In terms of the observed voltammetric peak potential, depending on the voltage scan rate (in the case of linear sweep voltammetry), this may shift either to give the illusion of greater or less electrochemical reversibility.

**Case B** This limit is that of a sub-monolayer of non-conductive particles on the surface of the substrate electrode at which the electron transfer necessarily occurs. Here the modified electrode acts as a 'partially blocked electrode' <sup>[6]</sup> with little analytical benefit.

**Case C** This case is that of a thick, porous layer of conductive particles <sup>[7]</sup> on a substrate electrode. If the layer is sufficiently substantial to obstruct diffusional analyte access to the latter, the modified electrode shows a response due to both the semi-infinite diffusion of the analyte from bulk solution to the surface of the porous layer (at which electrocatalytic effects of the modifier may operate) and due to electrolytic discharge within the pores of the layer. The latter often resembles that of thin layer diffusion <sup>[8]</sup> and the relative contributions of the two types of mass transport depend on the porosity of the modifying layer and its extent (thickness). The thin layer responses (noted in the case for some nanotube modified electrodes <sup>[8a]</sup>) have analytical value in that, in the case of electrochemically irreversible targets, the voltammetric peak potentials are shifted closer to the reversible formal potential of the redox couple of interest <sup>[8c]</sup>. That said in the case of close packed layers of nanoparticles the time response of the electrolysis of the occluded material is too short to be of value because of the tiny physical size of the pores leading to their very rapid depletion <sup>[7]</sup>.

**Case D** A sub-monolayer coverage of conductive particles on an electrode surface constitutes a 'spatially heterogeneous electrode' <sup>[9]</sup> and forms Case D. Analytically, it is desirable that the particles show a greater electro-catalytic activity than the substrate. In this case the average inter-particle separation,  $d$ , controls the observed voltammetry. Specifically, the response is clear in the light of the Einstein equation <sup>[10]</sup> for the distance diffused by an analyte in a certain time. It can be readily understood that if  $d \ll (6Dt)^{1/2}$ , where  $D$  is the analyte diffusion coefficient and  $t$  is the voltammetric timescale ( $t \sim RT/vF$ ;  $v$  is the voltage scan rate) then all the analyte diffusing to the geometric area of the electrode undergoes electrolysis at the particles. This, because of the catalytic properties of the particles, occurs at a lower potential than required on the less electro-catalytic substrate. Alternatively if  $d \gg (6Dt)^{1/2}$  the exposed areas of the substrate electrode contribute to the voltammetric response.

The purpose of the present paper is to explore aspects of the above limiting cases for two types of generic particles widely used in electroanalysis as possible electro-catalysts, namely nanoparticles and nanotubes (see Table 1). In both, we explore the extent to which drop casting can result in reproducible surfaces and the extent to which spatial heterogeneity is induced on the drop casted surface <sup>[11]</sup>.

**Table 1.** Illustrative recent works on detection using modified electrodes via the drop-casting of nanoparticles and nanotubes.

Name	Coating material	Electrode	Electrolyte	Analyte	Method	LOD	Sensitivity	Interference study (Y/N)	Ref.
Arduini F., <i>et al</i>	CB-AuNPs	SPE	0.1 M HCl + 0.01% AA	As(III)	ASV	0.4 ppb	673 $\mu\text{A } \mu\text{M}^{-1} \text{ cm}^{-2}$	Y	[12]
Jin L., <i>et al</i>	PtNP/CNT	GCE	0.1 M $\text{H}_2\text{SO}_4$	As(III)	LSV	0.12 ppb	0.70 $\text{A M}^{-1}$	N	[13]
Liu Y., <i>et al</i>	$\text{MnFe}_2\text{O}_4$ -AuNPs	GCE	0.1 M NaAc-HAc (pH = 5)	As(III)	SWASV	3.37 ppb	0.1 $\mu\text{A ppb}^{-1}$	Y	[14]
Abbas A., <i>et al</i>	MWCNT-Schiff base	CPE	B-R buffer solution (pH = 3.5)	Pd(II) Cd(II)	SWASV	1.2 x $10^{-4} \mu\text{M}$ 6.6 x $10^{-4} \mu\text{M}$	-	Y	[15]
Hong HG., <i>et al</i>	Nafion-MWCNT	GCE	1 M $\text{H}_2\text{SO}_4$	As(III)	ASV	0.75 ppb	4.76 $\mu\text{A } \mu\text{M}^{-1}$	Y	[16]
Majid KB., <i>et al</i>	Pb (IIP)	SPE	0.2M HCl	Pb(II)	DPV	3 ppm	49.179 $\text{nA/Nm}$	Y	[17]

Abbreviations: LOD: limit of detection; NP: nanoparticle; CB: carbon black; SPE: screen printed electrode; AA: acetic acid; ASV: anodic stripping voltammetry; CNT: carbon nanotube; GCE: glassy carbon electrode; LSV: linear sweep voltammetry; SWASV: square wave anodic stripping voltammetry; CPE: carbon paste electrode; B-R: Britton-Robinson; IIP: ion imprinted electrode; DPV: differential pulsed voltammetry.

## Experimental

**Reagents and instrumentation:** Pt nanoparticles ( $0.05 \text{ mg mL}^{-1}$ , 30 nm in diameter) dispersed in 2 mM sodium citrate were supplied by NanoComposix (San Diego, United States). Sodium (meta) arsenite ( $\text{NaAsO}_2$ , 99%) was purchased from Fluka (Buchs, Switzerland). Bamboo-like multi-walled carbon nanotubes (MWCNTs) of diameter ( $30 \pm 10$ ) nm and length (5-20)  $\mu\text{m}$  were purchased from Nanolab (Brighton, MA, USA). Sodium bromide (NaBr) was purchased from May and Baker (London, United Kingdom). Aqueous solutions were prepared using deionized water (Milipore, UK) with a resistivity of  $18.2 \text{ M}\Omega \text{ cm}$  at 298 K. The obtained materials were used without further purification.

Electrochemical measurements were conducted with a standard three electrode system in a Faraday cage at 298 ( $\pm 0.1$ ) K. Cyclic voltammetric measurements with PtNP modified GC electrode were recorded with an Autolab PGSTAT 30 computer-controlled potentiostat (EcoChemie, Netherlands) and CNT modified GC electrodes experiments were performed using  $\mu\text{Autolab II}$  potentiostat (Metrohm-Autolab BV, Utrecht, Netherlands). The computer software, GPES v.4.9 (Metrohm Autolab B.V., NL) was used to control and measure all electrochemical experiments. A glassy carbon electrode (GCE, diameter of 0.3 cm, geometric area of  $0.07 \text{ cm}^2$ , BAS technical, UK) served as a working electrode, and a graphite rod was applied as a counter electrode with a saturated calomel electrode (SCE, Radiometer, Copenhagen, Denmark) served as the reference electrode completed the three electrode system.

**Preparation of Pt nanoparticles modified GC electrodes:** The GC electrode was successively polished with 1  $\mu\text{m}$ , 0.3  $\mu\text{m}$  and 0.05  $\mu\text{m}$  sized alumina on a polishing pad then rinsed with deionized water prior to experiments. For drop casting with 0.05

$\mu\text{g}$  of PtNPs, the stock PtNP suspension was diluted first with 2 mM sodium citrate solution to  $0.01 \text{ mg mL}^{-1}$ , and sonicated for 1 min. Then  $5 \text{ }\mu\text{L}$  of diluted suspension was drop casted onto the electrode with micropipette and dried with a gentle  $\text{N}_2$  flow for 15 minutes. For drop casting with  $0.35 \text{ }\mu\text{g}$  of PtNPs, the  $7 \text{ }\mu\text{L}$  of stock suspension was directly drop casted onto the surface of GC electrode with a micropipette and dried with gentle  $\text{N}_2$  flow for 15 minutes.

The 30 nm Pt nanoparticles have been previously characterised by HR-CTEM<sup>[18]</sup> and shown to be an aggregate of much smaller nanoparticles of approximate diameter 3 nm (figure 2a) <sup>[18]</sup>. Such morphology is typical of Pt nanoparticles grown in the solution phase <sup>[18-19]</sup> and is potentially advantageous in the determination of arsenic because of their high active surface area <sup>[18-20]</sup>.

**Preparation of MWCNTs modified GC electrodes:** 1 mg of bamboo-like MWCNTs were dispersed in 1mL of acetone by sonicating it for 10 minutes. An aliquot of  $6 \text{ }\mu\text{L}$  and  $30 \text{ }\mu\text{L}$  of the MWCNTs dispersed was drop casted over polished glassy carbon electrode (GC) of diameter 0.3 cm. The modified GC electrode was dried under a constant gentle nitrogen gas flow for 15 minutes.

### **Optical microscopy and imaging:**

Optical measurements were made on a Zeiss Axio Examiner, A1 Epifluorescence microscope (Carl Zeiss Ltd., Cambridge U.K.) using a 10 $\times$  air objective (NA = 0.5, EC Plan-Neofluar). The light source was a LQ-HXP 120V lamp. In this study, the (epifluorescence) microscope used is that of a surface-reflective equivalent by removing the emission filter from the filter set (MDF-FITC  $475 \pm 35\text{nm}$ , Thorlabs). This allows a fraction of the incident light, reflected by the electrode surface, to be transmitted to the camera and thus allowing the surface of the opaque glassy carbon

electrode to be optically imaged. Image acquisition was provided by a black & white ORCA-Flash 4.0 digital CMOS camera (Hamamatsu, Japan), providing 16-bit images with 4-megapixel resolution.

### **Scanning Electron Microscopy:**

The Scanning Electron Microscopy (SEM) images were obtained using a Zeiss Sigma 300 FEG-SEM with an accelerating voltage of 2.0 kV. Prior to the measurements, the particles were suspended in water and drop-casted onto a cleaned glassy carbon stub, which was subsequently dried under vacuum.

### **Results and discussion**

In this section we present and discuss experimental results obtained first for the drop casting of an electrode with Pt nanoparticles and the use of the particle modified electrode (PME) for the detection of Arsenic (III) in aqueous solution. Second, we discuss the drop casting of carbon nanotubes to make PMEs for analytical voltammetry.

#### **(i) Platinum nanoparticles**

A Pt nanoparticle modified glassy carbon (GC) electrode was applied for Arsenic (III) detection. The nanoparticles were dispersed in an aqueous solution of 2 mM sodium citrate. A selected volume of the Pt nanoparticle suspension droplet (0.05  $\mu\text{g}$  to 15  $\mu\text{g}$  of Pt) was drop casted on the surface of GC electrode and dried with  $\text{N}_2$  flow. The Pt particles were aggregates of much smaller nanoparticles, which made them mesoporous and were capped by citrate <sup>[18]</sup>. According to the optical microscopy images shown in figures 2 c and d, a ring-like pattern was formed on the electrode surface after drop casting of Pt nanoparticles rather than a homogeneous structure.

The central part of the electrode was mostly, but not entirely, empty of particles so that when immersing into the analyte solution the latter directly contacted the bare electrode (figure 2b) and overall, the drop cast showed a clear so-called coffee ring pattern (figure 2 c1 and d1). The optical images shown in Figure 2 c1 and d1 are the surface of the GC electrode, taken directly after drop cast modification. The GC electrode was insulated by the polymer, polychlorotrifluoroethylene (PCTFE). Under the optical illumination used, the bright circular region of the image is the GC electrode, and this is surrounded by a black region which is the less reflective PCTFE polymer. In the case of the Pt nanoparticle modified electrode, drop cast directly from supplied suspension in citrate buffer solution, the volume of each drop casts leading to the corresponding mass of Pt residing on the GC electrode were finely controlled and optimised to ensure no overspill beyond the disk and onto the insulating plastic. Note that the aqueous droplet remains in the shape of a 'dome' on GC surface and does not spread out into the insulation plastic during evaporation.

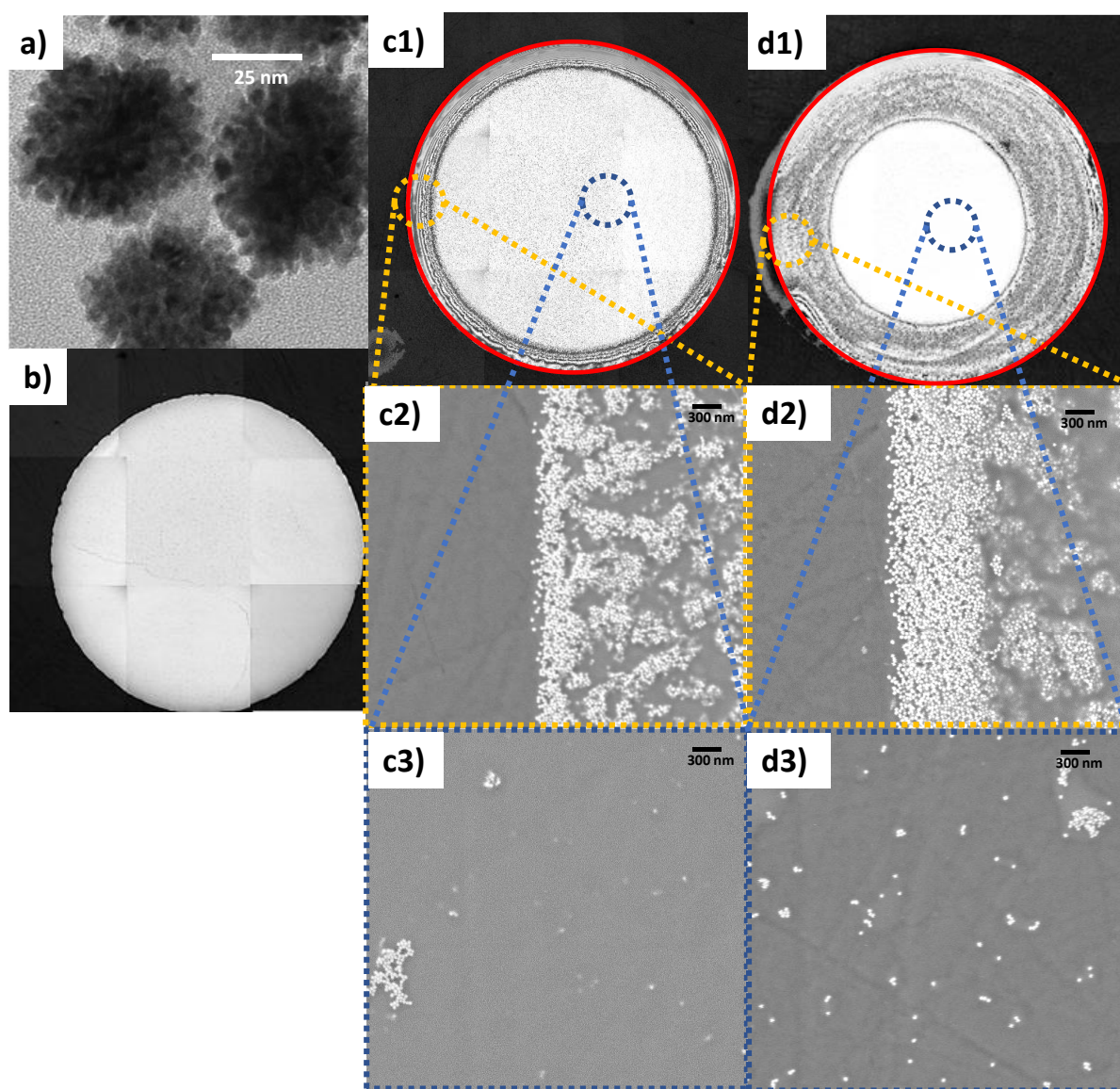


**Figure 2.** a) HR-CTEM image showing how the overall particle structure comprises of an aggregate of smaller substituent crystallites. Reprinted with permission from Yu *et al.* Copyright Royal Society of Chemistry 2019.<sup>[18]</sup> Images of b) bare GC electrode under optical microscope. c) 0.05  $\mu\text{g}$  of Pt nanoparticles modified GC electrode under optical microscope (c1), SEM images of Pt nanoparticles at the edge of the drop cast (c2) and SEM images of Pt nanoparticles at the centre of the drop cast (c3). d) 0.35  $\mu\text{g}$  of Pt nanoparticles under optical microscope (d1), SEM images at the edge of the drop cast (d2) and SEM image at the centre (d3). The areas within the red circle are electrode and others are the insulated material (c1 and d1). The geometric area of the GC electrode was  $0.07\text{ cm}^2$  and the average number of particles was  $1.6 \times 10^{10}$  particles  $\text{cm}^{-2}$ . The diameter of the PtNPs is 30 nm and dispersed in 2 mM sodium citrate solution. The scale bar of SEM images is 300 nm.

The coffee ring effect could occur when a sessile droplet containing suspended particles evaporated on a solid surface creating a ring-like pattern. This phenomenon was studied by Deegan *et al.*<sup>[21]</sup> and observed in the formation of coffee stains, where the rim of the stain was concentrated with particles while the centre had a much fewer

number of particles. This phenomenon has been labelled as the “coffee ring effect” (CRE).

One of the physical requirements to observe a CRE was the ‘pinning’ of the contact line at the edge or circumference of the droplet by surface tension forces <sup>[21-22]</sup>. The contact line pinning restricted the spreading and shrinking of the droplet during evaporation, and a radial outward capillary flow was observed towards the contact line since the evaporation flux at the edge was the greatest and a replenishment of solvent from centre is required. Thus, large number of particles were carried to the edge by the outward capillary flow, leading to the accumulation of an excess of particles at the periphery <sup>[23]</sup> as shown in figure 3. SEM images of the periphery of the drop cast showed large amounts of Pt nanoparticles and an ‘edge’ formed by particles was noticed (figure 2 c2 and d2), which was considered to be the location of the contact line <sup>[21]</sup>. SEM images were recorded to better observe the particle distributions on the surface of the modified electrodes, especially in the central particle deficient zone. A few particles were found to be randomly distributed in the central area (figure 2 c3 and d3). Note that whilst the (lower resolution) image from optical microscopy indicated an empty area in centre (figure 2 c1 and d1), on the basis of SEM, it contained a few distributed nanoparticles with separations depending on the mass of particles drop casted rather than none, in the case where 0.35  $\mu\text{g}$  were drop casted the particle-particles distances lay in the range between 300 to 800 nm. This is a key observation in the light of the discussion in the Introduction about the distances required between catalytic centres so that the diffusion fields associated with each overlap to cause diffusion to the full geometric area of the electrode.

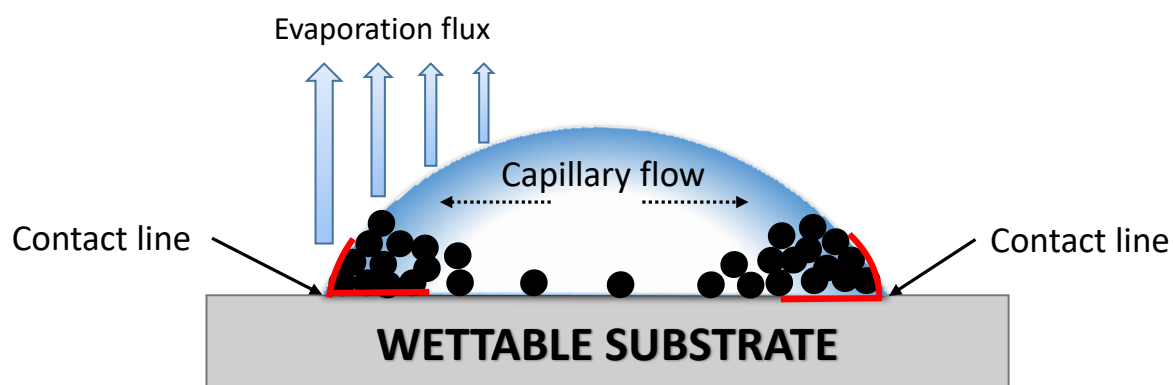


**Figure 3.** A scheme showing capillary flow from the centre to the edge of an evaporating droplet caused by the fixed contact line during evaporation. Particles in the droplet are moved to the edge by the induced capillary flow.

Note that a mass of  $0.05\ \mu\text{g}$  drop casted would correspond approximately to a coverage of 0.1 monolayers if the particles were to form a uniform close-packed layer. Clearly the particle deficient central zone has a much lower coverage of less than 0.1 monolayers reflecting the large number of particles were 'lost' to form the particle dense rings at the edge of the drop cast. Since these rings are composed of densely packed, electrically conducting, particles they are presumed to be in electrical contact with the substrate.

Having characterized the drop casted surfaces, next the analytical performances of the surfaces were investigated, using a  $1\ \text{mM}$  aqueous solution of sodium arsenite ( $\text{As(III)}$ ) in  $0.1\ \text{M}\ \text{H}_2\text{SO}_4$ . The Pt PME was then used for  $\text{As(III)}$  detection using cyclic voltammetry between  $+0.6\ \text{V}$  and  $+1.05\ \text{V}$ . Figure 4a shows cyclic voltammograms obtained from arsenic detection with PME of an area of  $0.07\ \text{cm}^2$  modified with between  $0.05\ \mu\text{g}$  to  $15\ \mu\text{g}$  of Pt nanoparticles of diameter  $30\ \text{nm}$ . The black curve represents the voltammogram measured from an electrode modified with  $0.05\ \mu\text{g}$  of Pt nanoparticles, and the red, green, blue, and cyan curve were  $0.35$ ,  $3.25$ ,  $7.5$ , and  $15\ \mu\text{g}$  of nanoparticles, respectively, and the surface coverages were equivalent to  $0.1$ ,  $0.754$ ,  $7.54$ ,  $15$  and  $30$  monolayers if the particles were to form a uniform close-

packed layer, which as seen above, they do not. In the voltammogram (figure 4a), a clear oxidative peak at +0.85 V (vs SCE) was observed and this was used to examine the analytical performance of the modified electrode. The peak was assigned to the two-electron oxidation of As(III) to As(V) [24].

The voltammograms as shown in figure 4b were analyzed first by means of Tafel analysis. The current analyzed were in the range of 10% to 30% of the peak currents [25]. The black, red, green, blue, and cyan points or line represent the 0.05, 0.35, 3.25, 7.5, and 15  $\mu\text{g}$  of Pt nanoparticles, respectively. The transfer coefficient,  $\beta$ , could be calculated based on Tafel law and the slopes in the Tafel plots in figure 4b, slope =  $\beta F/RT$ , where F is the Faraday constant, R is the ideal gas constant and T is the temperature. The transfer coefficient under room temperature was  $\sim 0.50$ , which indicates that the intermediate was formed in its electrical behaviour between the reactants and products.

Importantly the black line (0.05  $\mu\text{g}$ ) had smaller currents compared to other sets of data, which means the Pt nanoparticles were not sufficiently close together in some areas of the surfaces so as to allow for full diffusional overlap and to give the full diffusional response to arsenic expected for the geometric area of the electrode. This observation is entirely consistent with the data in figure 2c showing the Pt nanoparticles distributed poorly on the surface of the electrode and that the centre of the drop casted zone was deficient in Pt nanoparticles (figure 2 c3). Note that if the drop casted particles were uniformly distributed then an average surface coverage of 0.1 monolayers would lead to a calculated average particle separation of 2 microns which would be ample to achieve diffusional overlap and a voltammetric response reflecting diffusion to the geometric area of the electrode. For higher masses of drop

casted particles, from figure 4a that the voltammograms tended to a similar size and shape with roughly but not exactly consistent peak currents.

Figure 4c shows the peak current vs. the square root of scan rate of Pt PME's at the modified GCE with different amount of Pt nanoparticles (0.05  $\mu\text{g}$  - 15  $\mu\text{g}$ ). The black, red, green, blue, and cyan points or line represented the 0.05, 0.35, 3.25, 7.5, and 15  $\mu\text{g}$  of Pt nanoparticles, respectively. All sets of data points were linearly distributed and intercept approximately through the origin. The linear lines were aligned together except the black line, the 0.05  $\mu\text{g}$  data points, which means the Pt nanoparticles on the GC electrode were under a critical coverage and the response was not that of the geometric area.

The peak current data for the higher coverages (where fully diffusional overlap would lead to linear diffusion to the geometric area of the electrode) were analyzed using the irreversible Randles-Ševčík equation,

$$I_{peak} = 0.496 \sqrt{n' + \beta} nFA[A]_{bulk} \sqrt{\frac{FvD}{RT}} \quad (1)$$

where  $n'$  is electrons transferred in the rate-determining step,  $A$  is the geometric area of the electrode in  $\text{cm}^2$ ,  $\beta$  is the anodic transfer coefficient,  $[A]_{bulk}$  is the bulk concentration of the analyte in  $\text{mol m}^{-3}$ ,  $v$  is the scan rate in  $\text{V s}^{-1}$  and  $D$  is the diffusion coefficient in  $\text{cm}^2 \text{s}^{-1}$ .

The error bars shown in figure 4c were based on 3 experiments per point and confirm good reproducibility. Based on the Randles-Ševčík equation and the average slopes with high surface coverage in figure 4c, the diffusion coefficient was calculated to be  $9.7 \pm 0.3 \times 10^{-6} \text{ cm}^2 \text{s}^{-1}$  which was in good agreement with the literature value,  $1.0 \times 10^{-5} \text{ cm}^2 \text{s}^{-1}$  [26].

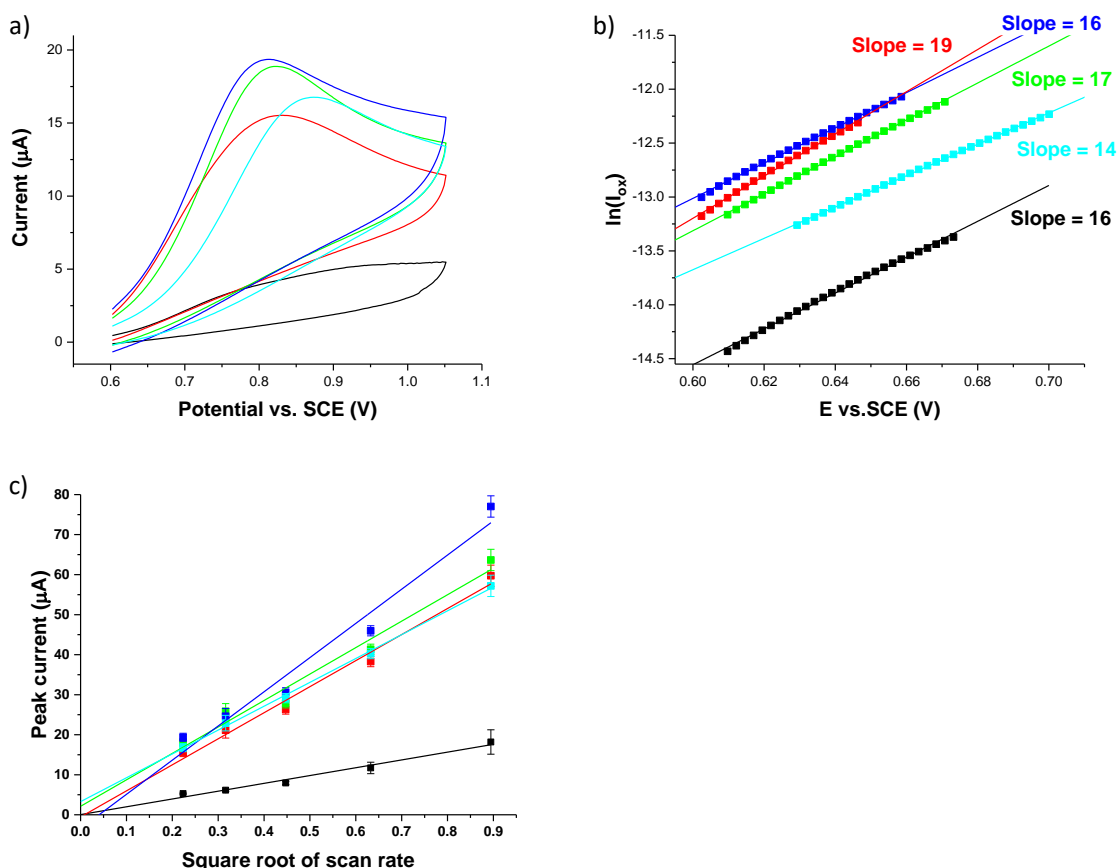


**Figure 4.** Plots of a) cyclic voltammograms, b) Tafel plots, and c) Randles–Ševčík plots of Pt PMEs containing 0.05 to 15  $\mu\text{g}$  of Pt nanoparticles. In all three plots, black, red, green, blue and cyan data points represented 0.05, 0.35, 3.25, 7.5, and 15  $\mu\text{g}$  of Pt nanoparticles. The measurements were conducted in 1 mM NaAsO<sub>2</sub> in 0.1 M H<sub>2</sub>SO<sub>4</sub> solution. GCE served as a working electrode, and a graphite rod was applied as a counter electrode with a SCE served as the reference electrode completed the three electrode system. The diameter of the PtNPs is 30 nm and dispersed in 2 mM sodium citrate solution.

It is interesting to note that the low coverage (equivalent to 0.1 monolayers) electrode produced a linear Randles–Ševčík response whilst obviously giving an erroneously low diffusion coefficient which was lower than half of the literature value. This observation indicates an essential need for drop casting to be supporting by imaging of the electrode surface especially if quantitative information is sought.

Last we note that for the red line (equivalent 0.75 monolayers) in figure 4c, an effectively full diffusional response was seen indicating a sufficient particle density in the central zone so as to ensure diffusional overlap such that all the active part of the electrode experiences linear (planar) diffusion. It is evident in the above that in order

to realise voltammetrically reliable reproducible surfaces, imaging of the drop cast is essential rather than relying on purely voltammetric indications since acceptable Randles- Ševčík plots albeit with erroneous slopes were obtained for partially covered surfaces. In the latter, the scaling of the peak current with the square root of scan rate reflects the existence of macroscopic patches of drop casted particles with the patch dimensions ( $d$ ) larger than  $(6Dt)^{1/2}$ . The imaging suggests that these patches are the annular zones forming the coffee ring pattern. The scope for voltammetric misinterpretation is evident. In order to further examine the surface heterogeneity effects on the voltammetry of drop casts attention was next turned to surfaces formed from casting carbon nanotubes.

## (ii) Carbon nanotubes

The electro-catalytic behaviour of drop casted multi-walled carbon nanotube modified electrodes was investigated in the context of aqueous bromide oxidation. The electrode was modified as following. The MWCNTs were first dispersed in acetone via 10 mins of sonication. 6  $\mu\text{g}$  and 30  $\mu\text{g}$  of the resulting solution was drop casted on clean and dried GC electrodes respectively. The geometric area of the GC electrode, was calculated to be 0.07  $\text{cm}^2$ . After drying the drop casted electrode with a constant nitrogen flow in a partially closed chamber, the MWCNTs drop casted GC electrodes were investigated using cyclic voltammetry to study MWCNTs as a possible electro-catalyst for the oxidation of bromide to bromine.

To characterize the deposition of the MWCNTs on the GC electrode, optical images were taken for the two PME and are shown in figure 5 (the contrast lines observed are due to the stitching series of the individually taken images and put together to form the full picture of a GC electrode). It was observed that the MWCNTs were deposited

on the GC electrode for both 6  $\mu\text{g}$  (figure 5a) and 30  $\mu\text{g}$  (figure 5b) but depending on the amount of aliquots drop casted, the active electrode area covered by the MWCNTs also varied. It is clear that no coffee ring pattern was observed yet a far from uniform deposit was created. For a drop cast of 6  $\mu\text{g}$ , the active electrode area covered by the MWCNTs was estimated to be ca. 20% and in the case of 30  $\mu\text{g}$  it was ca. 98%.

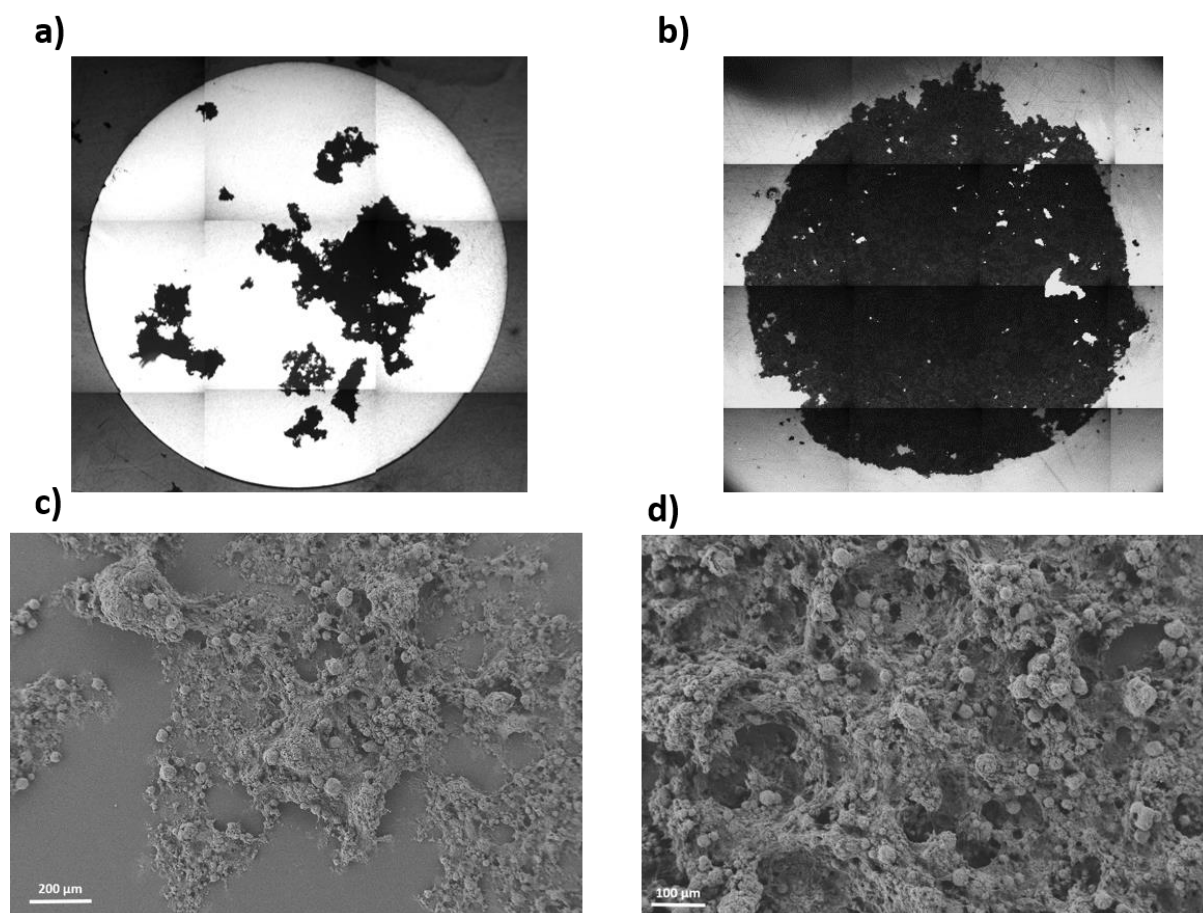


**Figure 5.** Images from optical microscope for a GC electrode with a geometric area 0.07 cm<sup>2</sup> which was drop casted with a) 6  $\mu\text{g}$  and b) 30  $\mu\text{g}$  of MWCNTs; c) and d) SEM images of 6  $\mu\text{g}$  MWCNTs drop casted over carbon slab.

However, in the latter case the deposit spread onto the insulation surrounding of the electrode; it is unclear to what extent the nanotubes in the latter area are in electrical contact with the substrate electrode. The extent to which the nanotubes aggregate and form multi-layered patches on the electrode is emphasized partly by the SEM images shown in figure 5c and d. If it is assumed that a MWCNT is a cylinder (length

20  $\mu\text{m}$  and diameter  $30 \pm 10 \text{ nm}$ ) when uniformly deposited with 6  $\mu\text{g}$  of drop cast in a close packed arrangement across the area of the electrode is calculated to have 25 layers of MWCNTs. Similarly for 30  $\mu\text{g}$  of drop casted MWCNTs (equivalent to 125 monolayers) if it is spread over the whole geometric area of the electrode. However, as shown in figure 5, they do not spread out uniformly but form macroscopic patches on the GC electrode. The absence of a coffee ring effect can be attributed to two major reasons. First, anisotropic 'particles' like MWCNTs exhibit strong long-range inter-particle attractions so that in contrast to spherical particles they form large clusters (as shown in figure 5 c and d) at the interface, on evaporation. As these clusters are large, their mobility towards the edge of the drop cast is restricted and the radially outward flow necessary for a coffee-ring effect to form is restricted. As a result, the MWCNTs are concentrated at the centre of the drop cast <sup>[27]</sup>. Second, Marangoni flows can be induced by volatile solvents such as acetone, as used in this case. A strong recirculating force can be created due to surface tension gradients and hence the suspended particles flow radially inward and settle at the centre of the drop cast <sup>[28]</sup>.

Based on the discussion in the Introduction of this paper the presence of macroscopic bare patches on the MWCNT modified electrodes is expected to influence the voltammetry observed at the electrode in the case of the low average coverages. In contrast the thicker layers formed at higher coverages may lack full electrical contact (both vertically and radially) throughout the film and can exhibit thin layer rather than semi-infinite diffusional effects [15].

To investigate these effects voltammetry of the oxidation of bromide to bromine was next undertaken. 5mM of NaBr dissolved in 0.1M of  $\text{HNO}_3$  was used as electrolyte for the investigation. The cyclic voltammogram as a function of scan rate is shown in figure 6 for the bare GC electrode. The oxidative peak was found to be at +1.12 V vs. SCE

(figure 6 black line) which is comparable to the literature value (+1.08 V vs. NHE) [29].

The peak to peak separation was of the order of several hundred mV and increased with scan rate which suggests that the oxidation of bromide in a GC electrode is fully electrochemically irreversible.

A plot of the peak current ( $I_p$ ) versus square root of scan rate ( $(V\ s^{-1})^{1/2}$ ) is given in figure 6b, the linearity shows that  $I_p$  is proportional to the square root of scan rate suggesting a diffusion-controlled process. The Randles–Ševčík equation (equation 1) for an irreversible one electron oxidation reaction was used to calculate the diffusion coefficient for the process using the measured transfer coefficient ( $\beta$ ) of 0.435 from the Tafel slope analysis and it was found to be  $2.12 \pm 0.0036 \times 10^{-5}\ cm^2\ s^{-1}$ .

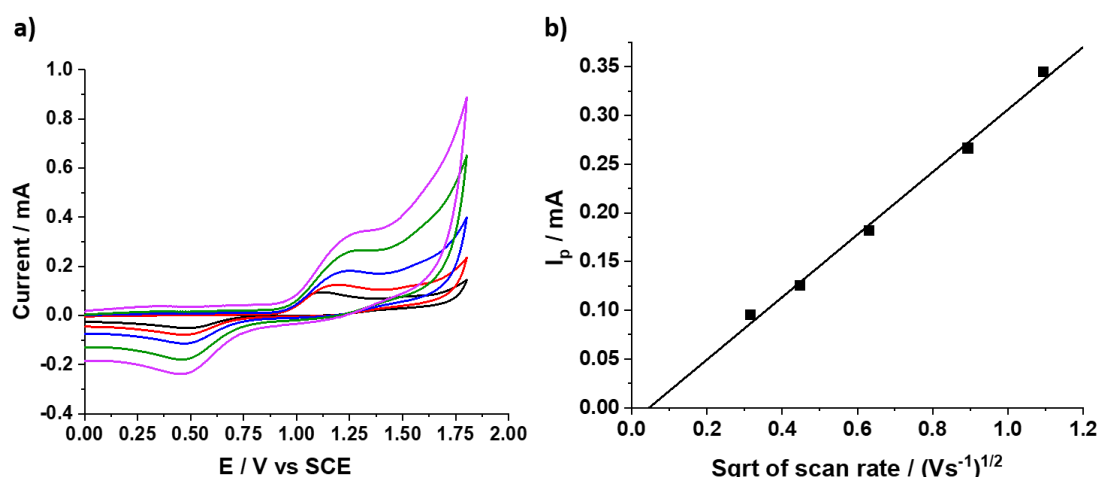


**Figure 6.** a) Voltammograms of a bare GC electrode in solution containing 5 mM NaBr + 0.1M  $\text{HNO}_3$  recorded as a function of scan rate (100  $\text{mV s}^{-1}$ , black line; 200  $\text{mV s}^{-1}$ , red line; 400  $\text{mV s}^{-1}$ , blue line; 800  $\text{mV s}^{-1}$ , green line; 1200  $\text{mV s}^{-1}$ , magenta line), b) a plot of peak current as a function of the square root of the scan rate from 100  $\text{mV s}^{-1}$  to 1200  $\text{mV s}^{-1}$ .

This value for the diffusion coefficient was independently checked using a platinum macro-electrode which gives reversible voltammetry under similar conditions (see SI figure 1).

The voltammetry for the bromide oxidation was then investigated on MWCNT-modified electrodes. The obtained voltammograms for the bare GC electrode, 25 monolayers drop cast (6  $\mu\text{g}$ ) and 125 monolayers drop cast (30  $\mu\text{g}$ ) at a scan rate of 200  $\text{mV s}^{-1}$  are shown in figure 7a.

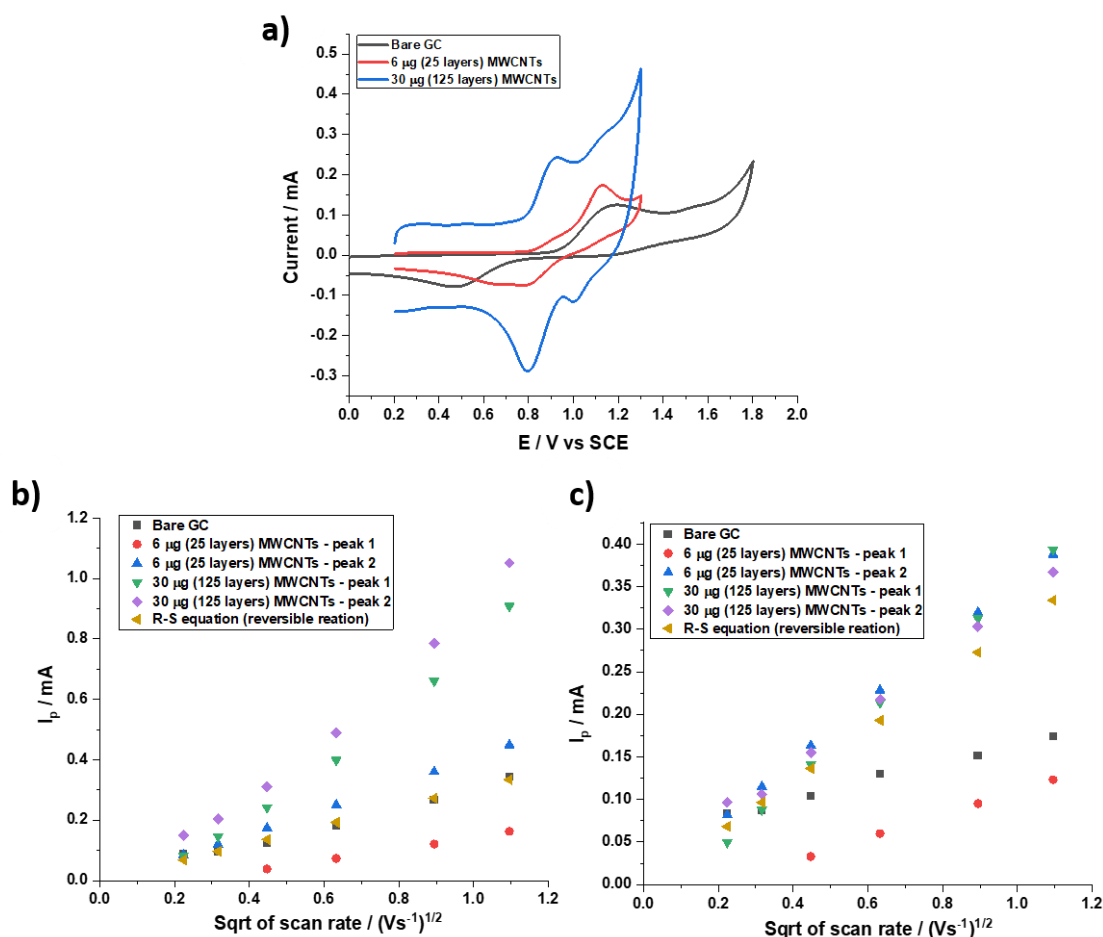


**Figure 7.** (a) Cyclic voltammograms of bare GC, black line; 6  $\mu\text{g}$  drop cast of MWCNTs (25 monolayers), red line and 30  $\mu\text{g}$  drop cast of MWCNTs (125 monolayers), blue line at a scan rate of 0.2  $\text{V s}^{-1}$ . Plots of peak current  $I_p$  vs square root of scan rate (b) before and (c) after background subtraction. The analysed solution was 5 mM NaBr in 0.1 M  $\text{HNO}_3$ .

The plot of peak current vs square root of scan rate shows the comparison between the peak currents of bare GC, 25 monolayers (6  $\mu\text{g}$ ), 125 monolayers (30  $\mu\text{g}$ ) and the estimated peak current using Randles–Ševčík equation for a reversible one electron transfer process. Figure 8a shows the raw data without any background subtraction

and figure 8b is the voltammograms after background subtraction for all the experimental voltammograms obtained.

In the case of the lower coverage of nanotubes where the microscopy reported above shows a heterogeneous surface comprised of bare patches of electrodes and patches of heavily agglomerated nanotubes, it can be seen that the peak potentials of both the oxidative and reductive features shift closer together in comparison to the bare electrode. For the higher coverage both peaks have shifted much closer together and the voltammetric response (figure 7a) is apparently more reversible although a very significant background current is observed as a result of capacitive charging as evidenced by the currents flowing in the potential range 0.2 – 0.6 V. The voltammograms as a function of scan rate for the MWCNTs deposited GC electrode is shown in figure 8 (a and c are voltammograms before background subtraction; b and d are respective voltammograms after background subtraction). The current-potential response for 0.1M HNO<sub>3</sub> was obtained and was used as background to subtract the capacitive charging from the actual voltammogram obtained for bromide oxidation and is shown in figures 8 b and c. The latter (30 µg) indicates a much greater electrode-electrolyte interfacial area as compared to the bare electrode and shows that the patches of agglomerates are likely highly porous. Interestingly the low coverage voltammogram (figures 8 a and b) shows a pre-wave of electroactivity at the potentials at which the bromide oxidation is seen for the higher coverage (figures 8 c and d). Accordingly the response is that of a mixed surface – bare patches of GC and porous patches of agglomerated particles was observed.

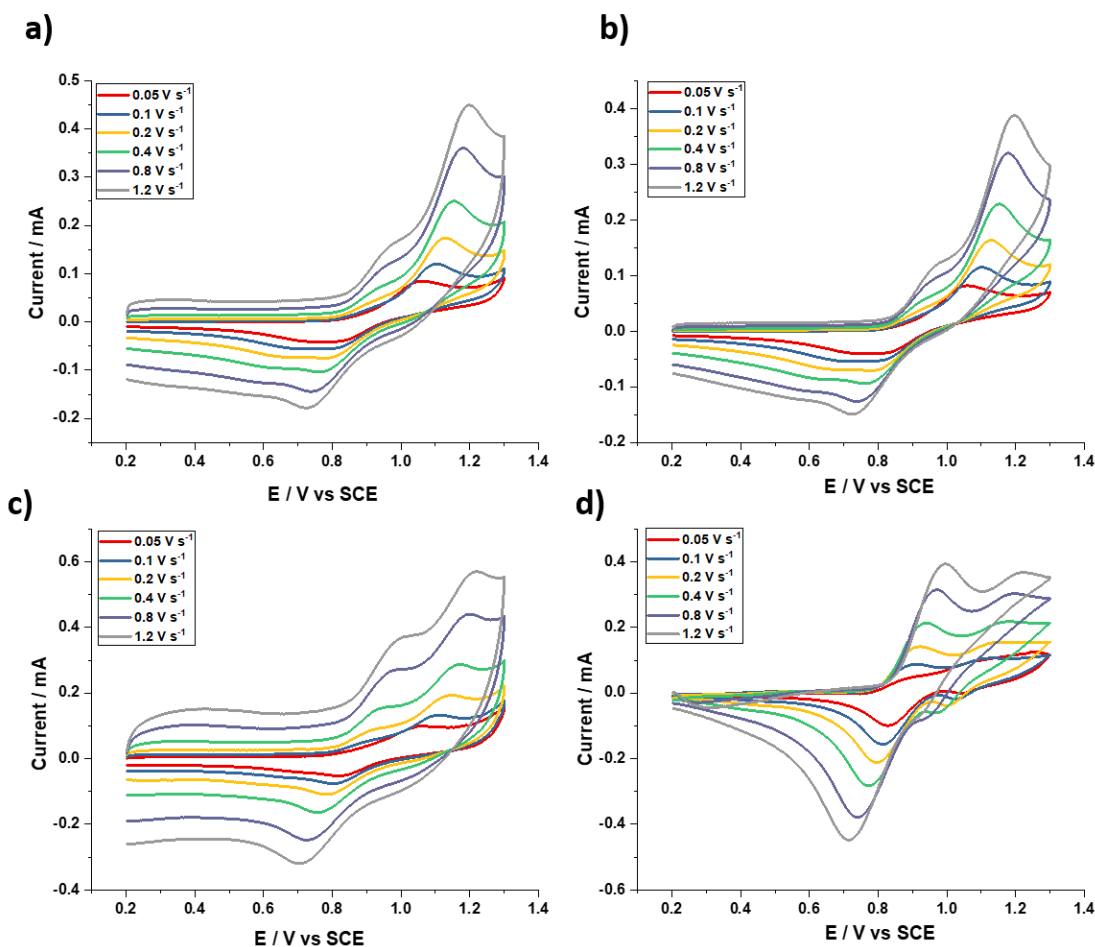


**Figure 8.** Cyclic voltammograms on a 6  $\mu\text{g}$  of MWCNTs modified GC electrode (a) before background subtraction (b) after background subtraction and 30  $\mu\text{g}$  of MWCNTs (c) before background subtraction (d) after background subtraction (50  $\text{mV s}^{-1}$ , red line; 100  $\text{mV s}^{-1}$ , blue line; 200  $\text{mV s}^{-1}$ , yellow line; 400  $\text{mV s}^{-1}$ , green line; 800  $\text{mV s}^{-1}$ , navy line; 1200  $\text{mV s}^{-1}$ , grey line). The analysed solution was 5 mM NaBr in 0.1 M  $\text{HNO}_3$ .

The change in the apparent electrochemical reversibility of the bromide oxidation in the presence of the CNTs might at first sight signal ‘electro-catalysis’ because of the increased apparent reversibility. However, the effect is equally consistent with the expected ‘thin-layer’ like voltammetry expected for porous layers. The CNTs exhibit a complicated mass transport behaviour which mostly is a combination of thin-layer and semi-infinite diffusion <sup>[30]</sup>. Figure 9 shows a logarithmic plot of peak current vs scan rate before (figure 9a) and after (figure 9b) background correction. The gradient value for each linear plot was found to deviate from 0.5, which corresponds to semi-infinite diffusion and the value of 1 which is expected for thin layer diffusion and/or adsorbed

species <sup>[30a]</sup>. This indicates that a mixed mass transport regime is observed with a combination of first thin layer diffusion (or an adsorptive response) observed in the interior of the MWCNTs layer and second semi-infinite diffusion to the surface of the layer <sup>[31]</sup>. The high surface area of the MWCNTs can facilitate the adsorption of the electroactive species which makes it difficult to unambiguously distinguish between thin layer effects and the adsorption effects <sup>[30b, 32]</sup>.

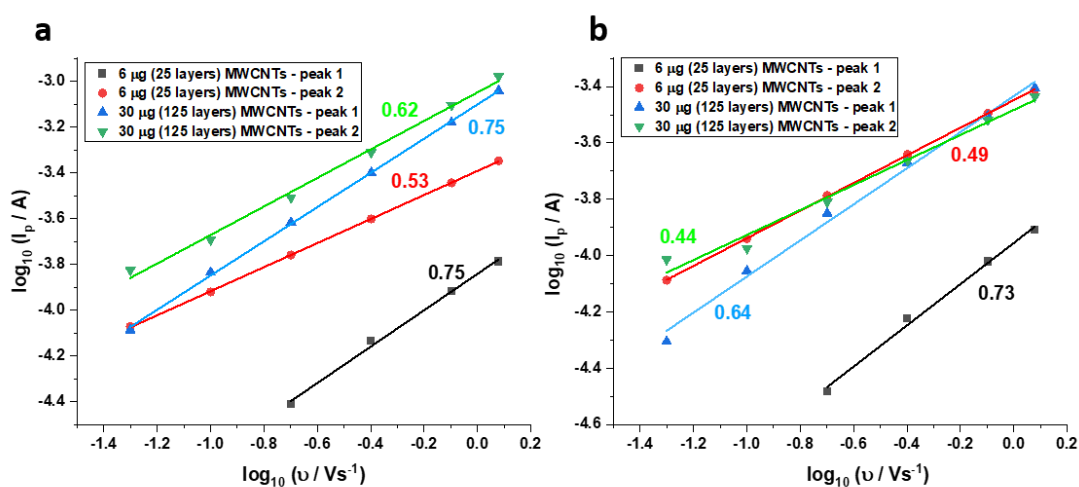


**Figure 9.** The logarithmic plot of peak current  $I_p$  vs scan rate (a) before background subtraction with gradients of 0.75 for 6  $\mu\text{g}$  of MWCNTs - peak 1 (square, black line), 0.53 for 6  $\mu\text{g}$  MWCNTs - peak 2 (circle, red line), 0.75 for 30  $\mu\text{g}$  MWCNTs - peak 1 (upward triangle, blue line), 0.62 for 30  $\mu\text{g}$  MWCNTs - peak 2 (downward triangle, green line) (b) after background subtraction with gradients of 0.73 for 6  $\mu\text{g}$  MWCNTs - peak 1, 0.49 for 6  $\mu\text{g}$  MWCNTs - peak 2, 0.64 for 30  $\mu\text{g}$  MWCNTs - peak 1, 0.44 for 30  $\mu\text{g}$  MWCNTs - peak 2. The analysed solution was 5 mM NaBr in 0.1 M  $\text{HNO}_3$ .

## Conclusions

Drop-casting is a widely used method for the creation of PMEs, especially for electroanalysis. Often the creation of a random distribution of particles is assumed and this can be encouraged by electrochemical responses which are not inconsistent with the presumed surface morphology. However it is clear that drop casts which are far from ideal can be formed with Pt nanoparticles forming coffee rings and MWCNTs forming a patch surface with exposed areas of bare electrode. Since both types of surface give

plausible voltammetric responses it is evident that complementary microscopic imaging must be conducted in parallel with the electrochemistry in order to obtain to avoid erroneous conclusions both qualitative and quantitative.

## Acknowledgements

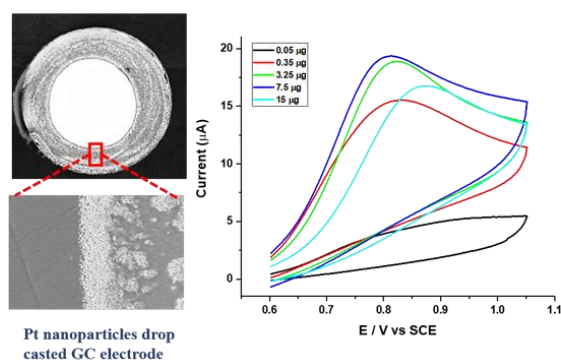
Archana K. S thanks the Commonwealth Scholarships Commission UK and University of Oxford for funding her DPhil. D. Li thanks the China Scholarship Council and the University of Oxford for supporting her D.Phil studies. M.Y. acknowledges funding via the EPSRC Industrial CASE award EP/N509711/1.

## References

- [1] aC. Xue, Q. Han, Y. Wang, J. Wu, T. Wen, R. Wang, J. Hong, X. Zhou, H. Jiang, *Biosens. Bioelectron.* **2013**, *49*, 199-203; bS. Alim, J. Vejayam, M. M. Yusoff, A. Kafi, *Biosens. Bioelectron.* **2018**, *121*, 125-136; cE. Asadian, M. Ghalkhani, S. Shahrokhian, *Sens. Actuators, B* **2019**, *293*, 183-209; dF. W. Campbell, R. G. Compton, *Anal. Bioanal. Chem.* **2010**, *396*, 241-259; eJ. M. George, A. Antony, B. Mathew, *Microchim. Acta* **2018**, *185*, 358.
- [2] G. Zhao, Y. Lin, K. Rui, Q. Zhou, Y. Chen, S. X. Dou, W. Sun, *Nanoscale* **2018**, *10*, 19074-19081.
- [3] J. Stacy, Y. N. Regmi, B. Leonard, M. Fan, *Renewable Sustainable Energy Rev.* **2017**, *69*, 401-414.
- [4] S. Eloul, R. G. Compton, *J. Phys. Chem. C* **2014**, *118*, 24520-24532.
- [5] aL. Chen, E. Kätelhön, R. G. Compton, *Appl. Mater. Today* **2019**, *16*, 141-145; bE. Kätelhön, L. Chen, R. G. Compton, *Appl. Mater. Today* **2019**, *15*, 139-144; cL. Chen, E. Kätelhön, R. G. Compton, *Appl. Mater. Today* **2020**, *18*, 100480.
- [6] B. A. Brookes, T. J. Davies, A. C. Fisher, R. G. Evans, S. J. Wilkins, K. Yunus, J. D. Wadhawan, R. G. Compton, *J Phys Chem B* **2003**, *107*, 1616-1627.
- [7] E. Kätelhön, R. G. Compton, *Appl. Mater. Today* **2020**, *18*, 100514.
- [8] aM. J. Sims, N. V. Rees, E. J. Dickinson, R. G. Compton, *Sens. Actuators, B* **2010**, *144*, 153-158; bI. Streeter, G. G. Wildgoose, L. Shao, R. G. Compton, *Sens. Actuators, B* **2008**, *133*, 462-466; cM. C. Henstridge, E. J. Dickinson, M. Aslanoglu, C. Batchelor-McAuley, R. G. Compton, *Sens. Actuators, B* **2010**, *145*, 417-427.
- [9] T. J. Davies, R. R. Moore, C. E. Banks, R. G. Compton, *J. Electroanal. Chem.* **2004**, *574*, 123-152.
- [10] A. Einstein, *Ann. Phys.* **1905**, *17*, 208.
- [11] H. Li, D. Buesen, R. Williams, J. Henig, S. Stapf, K. Mukherjee, E. Freier, W. Lubitz, M. Winkler, T. Happe, *Chem. Sci.* **2018**, *9*, 7596-7605.
- [12] S. Cinti, S. Politi, D. Moscone, G. Palleschi, F. Arduini, *Electroanalysis* **2014**, *26*, 931-939.
- [13] H. Xu, L. Zeng, S. Xing, Y. Xian, L. Jin, *Electrochem. Commun.* **2008**, *10*, 551-554.
- [14] S. Zhou, X. Han, H. Fan, Y. Liu, *Sensors* **2016**, *16*, 935.
- [15] A. Afkhami, H. Ghaedi, T. Madrakian, M. Rezaeiavala, *Electrochim. Acta* **2013**, *89*, 377-386.
- [16] S.-H. Shin, H.-G. Hong, *Bull. Korean Chem. Soc.* **2010**, *31*, 3077-3083.

- [17] M. K. Bojdi, M. H. Mashhadizadeh, M. Behbahani, A. Farahani, S. S. H. Davarani, A. Bagheri, *Electrochim. Acta* **2014**, *136*, 59-65.
- [18] W. Yu, C. Batchelor-McAuley, X. Chang, N. P. Young, R. G. Compton, *Phys. Chem. Chem. Phys.* **2019**, *21*, 20415-20421.
- [19] X. Jiao, C. Batchelor-McAuley, C. Lin, E. Kätelhön, E. E. Tanner, N. P. Young, R. G. Compton, *ACS Catal.* **2018**, *8*, 6192-6202.
- [20] X. Jiao, S. V. Sokolov, E. E. Tanner, N. P. Young, R. G. Compton, *Phys. Chem. Chem. Phys.* **2017**, *19*, 64-68.
- [21] R. D. Deegan, O. Bakajin, T. F. Dupont, G. Huber, S. R. Nagel, T. A. Witten, *Nature* **1997**, *389*, 827-829.
- [22] R. D. Deegan, *Phys. Rev. E* **2000**, *61*, 475.
- [23] H. Eral, J. Oh, *Colloid Polym. Sci.* **2013**, *291*, 247-260.
- [24] aT. D. Cabelka, D. S. Austin, D. C. Johnson, *J. Electrochem. Soc.* **1984**, *131*, 1595; bX. Dai, R. G. Compton, *Analyst* **2006**, *131*, 516-521.
- [25] D. Li, C. Lin, C. Batchelor-McAuley, L. Chen, R. G. Compton, *J. Electroanal. Chem.* **2018**, *826*, 117-124.
- [26] D. G. Williams, D. C. Johnson, *Anal. Chem.* **1992**, *64*, 1785-1789.
- [27] P. J. Yunker, T. Still, M. A. Lohr, A. G. Yodh, *Nature* **2011**, *476*, 308-311.
- [28] H. Hu, R. G. Larson, *J Phys Chem B* **2006**, *110*, 7090-7094.
- [29] W. Haynes, *CRC Handbook of Chemistry and Physics 93RD Edition*, 2012, CRC Press, New York, **2012**.
- [30] aM. J. Sims, N. V. Rees, E. J. F. Dickinson, R. G. Compton, *Sensor Actuat B-Chem* **2010**, *144*, 153-158; bY. Y. Chan, A. Y. Eng, M. Pumera, R. D. Webster, *ChemElectroChem* **2015**, *2*, 1003-1009.
- [31] I. Streeter, G. G. Wildgoose, L. D. Shao, R. G. Compton, *Sensor Actuat B-Chem* **2008**, *133*, 462-466.
- [32] M. C. Henstridge, E. J. F. Dickinson, M. Aslanoglu, C. Batchelor-McAuley, R. G. Compton, *Sensor Actuat B-Chem* **2010**, *145*, 417-427.

## Table of contents



An overlay of cyclic voltammetry is employed for the comparison of the coffee ring effect on drop cast of Pt nanoparticles. Although most of the particles were agglomerated at the edge of the electrode due to the coffee ring effect, the CV of the determination of arsenic was not affected if enough amount of Pt nanoparticles were applied.